Bandgap-tailored NiO nanospheres: an efficient photocatalyst for the degradation of crystal violet dye solution

Raja Vahini[1] · Puvaneswaran Senthil Kumar[1] · Swaminathan Karuthapandian[1]

Abstract Bandgap-tailored NiO nanospheres were successfully synthesized by facile precipitation method for the first time and characterized by XRD, EDX, SEM, TEM, FTIR, UV and PL. Interestingly, the modification of the band gap was observed using UV–Vis (DRS) spectroscopy, and the observed band gap is 3.31 eV. The morphology of the materials was analysed by SEM and TEM which show the sphere like structures of NiO with the particle size of ~ 20 nm. The efficiency of the materials was examined by the degradation of crystal violet dye under UV light illumination. The complete degradation was achieved within 60 min, and the mechanism of the degradation were also been proposed. In addition, the degradation of rhodamine B (RhB) and methylene blue dye solution was also carried out to extend the practical applications of NiO nanospheres. The involvement of reactive oxidative species (ROS) was found out by trapping experiment, and the ROS is superoxide radical anion.

1 Introduction

Industrial wastewater usually contains a variety of harmful organic compounds and toxic substances, and it causes the most serious environmental problems [1–4]. It is estimated

✉ Swaminathan Karuthapandian
   drpandianskvhnsnc2007@gmail.com

1   Department of Chemistry, VHN Senthikumara Nadar
    College, Virudhunagar, Tamilnadu 626 001, India

that around 700,000 tons of dyes were produced annually around the world [5]. The paper, leather, cosmetic and food industries are the major consumers for various types of triphenylmethane dyes [6]. Crystal violet (CV) is a typical triphenylmethane dye used as a biological stain or dermatological agent [7, 8]. The wide use of CV dye for different application caused the presence of this substance in waste streams and disposal wastewater [9–11]. Since this compound was characterized as a toxic agent [12–14], its elimination through transformation into non-hazardous species using different semiconductors was a demanding area of research. Traditional treatments including coagulation/flocculation, membrane separation, activated carbon adsorption and biological treatment were not been able to remove 100 % of the dye from waste streams efficiently [15–18].

Consequently, finding other effective treatment technologies seemed to be necessary. Advanced oxidation process (AOP), a photo-catalytic reaction, is a promising and emerging process which attracted globally for the degradation of organic pollutants through the intersession of photo energy, employing a suitable semiconductor photocatalyst [19, 20]. The efficiency of the catalyst for the treatment of effluents loaded with different dyes is a critical task. Hence, our research focused on the treatment of organics through photocatalysis reaction pathway. NiO is a p-type semiconductor with a wide bandgap material (3.45–4.5 eV) valence band [3.1 eV] suitable for photocatalytic processes [21–23]. Nevertheless, the application of CuO was wide and broad until now; however, in most reports, NiO was used only as a sensitizer of a composite photocatalyst. There are a very few reports available for the NiO used solely as a photocatalyst [24, 25]. Furthermore, the bandgap-altered NiO without using any external supports, materials and dopants has not been yet reported.

Nevertheless, to the best of our knowledge, until now, there are a very few reports available on the synthesis of band-gap-tailored NiO.

Hence, we made an attempt for the simple synthesis of bandgap-tailored NiO nanospheres for the first time and used as a photocatalyst for the degradation of triphenylmethane dye for the very first time. The as-synthesized NiO nanospheres are characterized by XRD, EDAX, PL, FTIR, DRS UV–Vis, SEM and TEM. Triphenylmethane [crystal violet (CV)] dye was targeted as the probe pollutant for the evaluation of photocatalytic efficiency of as-synthesized NiO nanospheres under UV light illumination. In addition, the degradation of rhodamine B (RhB) and methylene blue (MB) dye solution was also carried out to extend the practical applications of NiO nanospheres. Based on the trapping experimental results, a possible mechanism for the enhanced photocatalytic activity of NiO nanospheres is also proposed.

2 Experimental methods

All the chemicals were purchased from the Merck chemicals, India, and used as such without any further purification. Deionized water was used throughout the experiment. Detailed experimental protocols were given as supplementary information.

3 Results and discussion

3.1 Structural analysis

The crystalline phase and crystalline nature of the as-synthesized NiO nanospheres were studied by XRD analysis which is shown in Fig. 1a. The diffraction peaks of NiO

nanospheres are indexed as cubic phase and well matched with the standard JCPDS card 89-7130. The observed diffraction patterns of NiO nanospheres were found in the 2θ regions of $37.30°$, $43.32°$, $63.04°$, $75.49°$ and $79.71°$, which correspond to the reflection planes of (111), (200), (220), (311) and (222), respectively. The sharp and high intensity of the diffraction peaks of NiO nanospheres was clearly indicated the high crystallinity. It was observed that the (200) reflection of plane was the preferred orientation, and the NiO nanospheres was grown in the (200) direction. The average crystallite size was calculated using the Scherrer equation, and the crystallite size (D) were calculated for the (200) reflection plane is 44 nm. Dislocation density (d) is defined as the number of dislocation lines per unit volume of the crystal, and its value is calculated by using Eq. (1) [26].

$$\delta = \frac{1}{D^2} \tag{1}$$

The calculated dislocations per line for NiO nanospheres were 5.16×10^{-14} m^{-2}, and this clearly indicates some sort of dislocations per line. The 5.16×10^{-14} m^{-2} dislocations per line might be due to the peak shift in the XRD pattern.

The structural information of the NiO nanospheres was further confirmed by the FTIR analysis which is shown in Fig. 1b. In general, the stretching vibration band in the range of $400–600$ cm^1 was attributed to M–O bonds (metal–oxide). The stretching vibration band appeared at 470 and 521 cm^{-1} was due to the Ni–O bond [27]. The stretching vibration bands observed at 1020, 1383 and 1648 cm^{-1} were assigned to the stretching mode of O–O bond and stretching vibration of C–C bond, respectively. The bands except Ni–O appeared in the FTIR spectrum might be formed due to the presence of trace level organic impurity which is used in the synthesis experiments. No
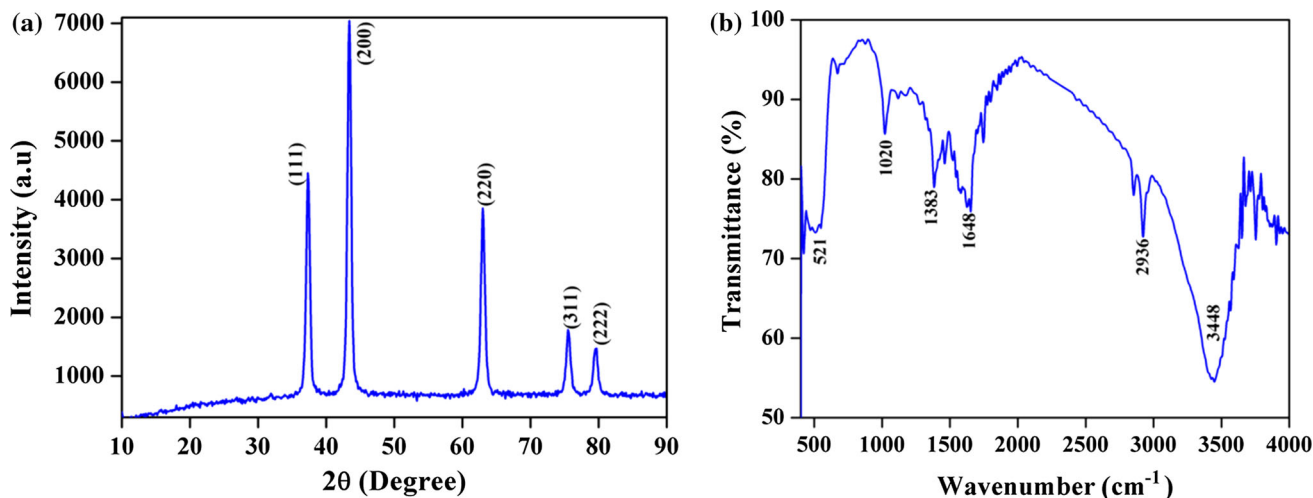

Fig. 1 a XRD patterns of as-synthesized NiO nanospheres and b FTIR spectrum of as-synthesized NiO nanospheres

other bands are observed in the FTIR spectra which confirm that only metal oxygen functional groups are present.

3.2 Morphological analysis

The morphology of the as-synthesized NiO nanospheres was analysed by SEM which is shown in Fig. 2a, b. SEM micrographs of NiO nanospheres showed that the microspheres with little aggregation and the average particle size are 500 nm. The surface of the NiO also looked like significantly porous. Figure 2b is the enlarged image of Fig. 2a which showed the smooth and sponge like surface. The presence of nickel and oxide was confirmed by the EDX analysis which is shown in Fig. 2c. Nickel was present about 55 %, and Oxygen was present about 44 % which clearly indicated the formation of NiO nanospheres. It is evident from EDX spectra that there are no other elemental peaks other than nickel and oxygen was observed which clearly indicated the purity of as-synthesized NiO nanospheres.

The surface morphology and particle size of as-synthesized NiO nanospheres were further evidenced by TEM analysis which is shown in Fig. 3. Interestingly, TEM images showed that the more number of spherically sphere particles and some hexagonal like particles was observed (Fig. 3a). Figure 3b, c clearly showed the individual spherically sphere and hexagonal particle with the particle size of 5 nm. To make it clear and better sounds, we have named as NiO nanospheres because the presence of more number of spheres. The lattice fringes of as-synthesized NiO nanospheres were showed the (200) orientation (Fig. 3d), and the results are in line with the XRD results.

3.3 Optical properties

The UV–visible spectroscopy is one of the most efficient techniques employed for the investigation of optical properties of the semiconductor materials. The absorption spectrum of NiO nanospheres are shown in Fig. 4. It can be seen that the absorbance of NiO nanospheres falls in the UV region and the absorption steep at 250–500 nm which corresponds to the bandgap energy of NiO nanospheres. The bandgap energy (E_g) of the nanospheres was calculated using the formula (Eq. 2)

$$(\alpha) = \frac{A}{hv(hv - E_g)^{-1/2}} \tag{2}$$

where α is the absorption coefficient in cm^{-1}, hv is photon energy in eV, A is a constant which is related to the effective masses associated with valence band and conduction band, and E_g is the gap between the bottom of the conduction band and top of valence band at the same value of the wave vector. From the calculated value of absorption coefficient, a plot of (hv) versus $(\alpha hv)^2$ was drawn. Extrapolation of the linear portion of the graph to the energy (hv) axis gives the bandgap value of the NiO nanospheres as shown in Fig. 4b. The bandgap value of the NiO nanospheres in the present work is found to be 3.31 eV. In general, NiO has the bandgap value of around 3.4–4.5 eV. Interestingly, the band gap of prepared NiO nanospheres is 3.31 eV which is rather wider than the commercial one [28].

3.4 Photocatalytic activity

The photocatalytic activity of the as-synthesized NiO was evaluated towards the degradation of CV dye solution under UV light irradiation. Figure 5a showed the absorption spectra of CV solution with different time intervals, and the characteristic absorption peak at 582 nm of CV solution was continuously decreased. After 60 min of irradiation, the characteristic peaks of CV dye solution were decreased drastically. Moreover, C/C_0 (C_0—initial concentration of CV solution, C—concentration of CV solution at time intervals) was plotted against the irradiation time which confirmed the complete mineralization of pollutant. There was no degradation of CV dye solution that was observed in the absence of catalyst as well as in
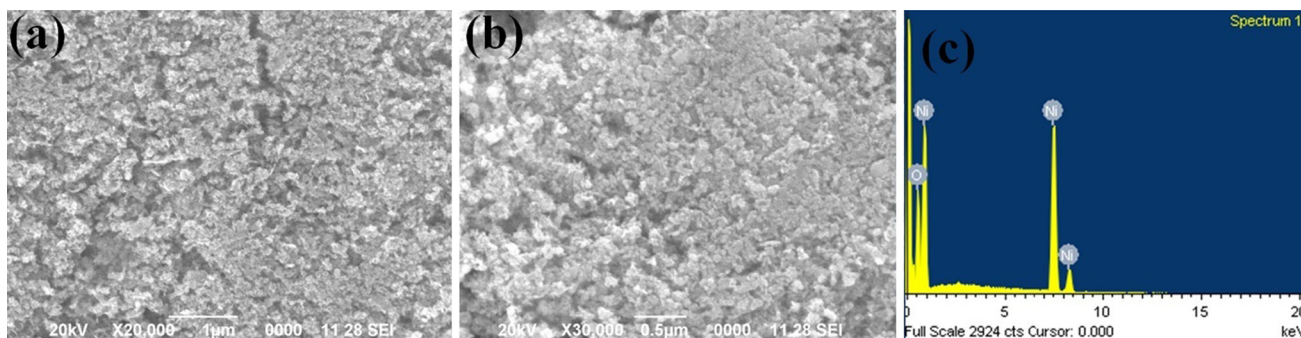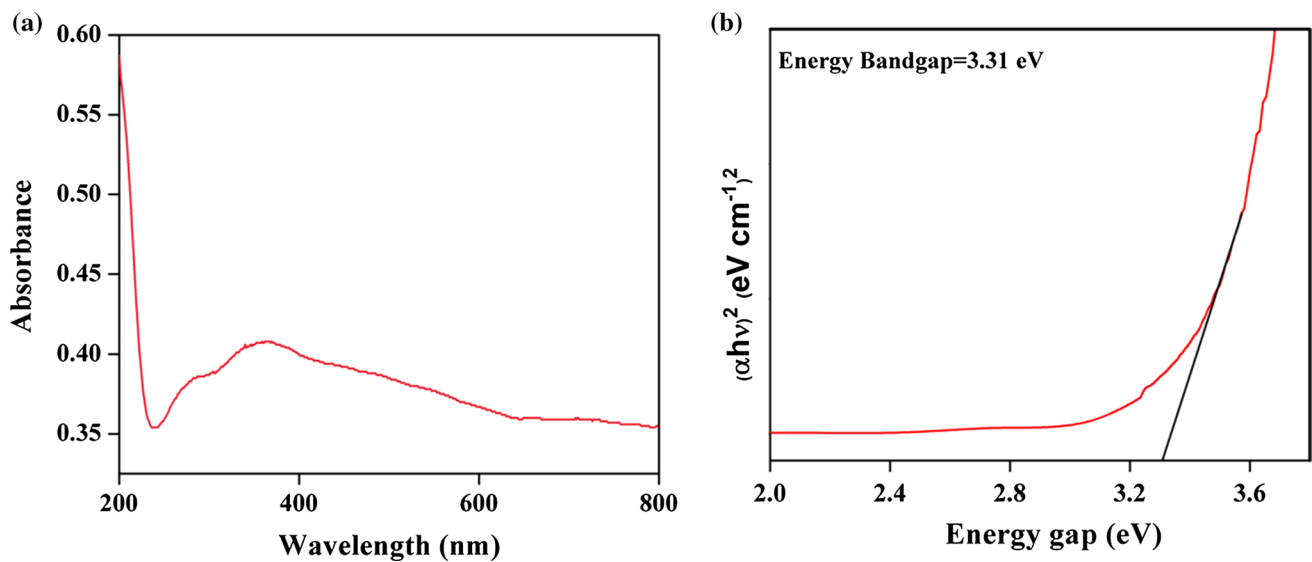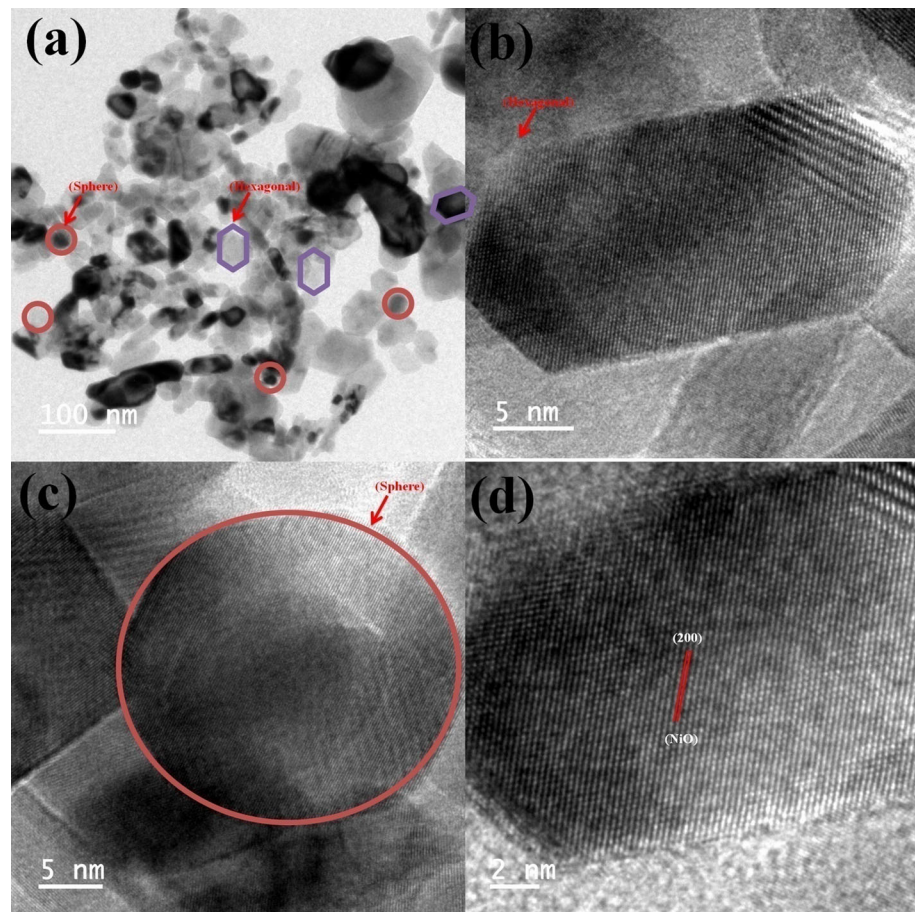

Fig. 2 **a**, **b** SEM micrographs of as-synthesized NiO nanospheres and **c** EDX spectrum of as-synthesized NiO nanospheres

Fig. 3 TEM images of as-synthesized NiO nanospheres

Fig. 4 **a** Absorption spectrum of as-synthesized NiO nanospheres **b** Energy gap of NiO nanospheres

absence of light. It was clearly indicated that as-synthesized NiO nanospheres and light sources are essential for the photodegradation reaction. Furthermore, the photocatalytic degradation of RhB and MB dye solution was carried out to extend the potential applications of NiO nanospheres as illustrated in Fig. 5b, c. Interestingly, the
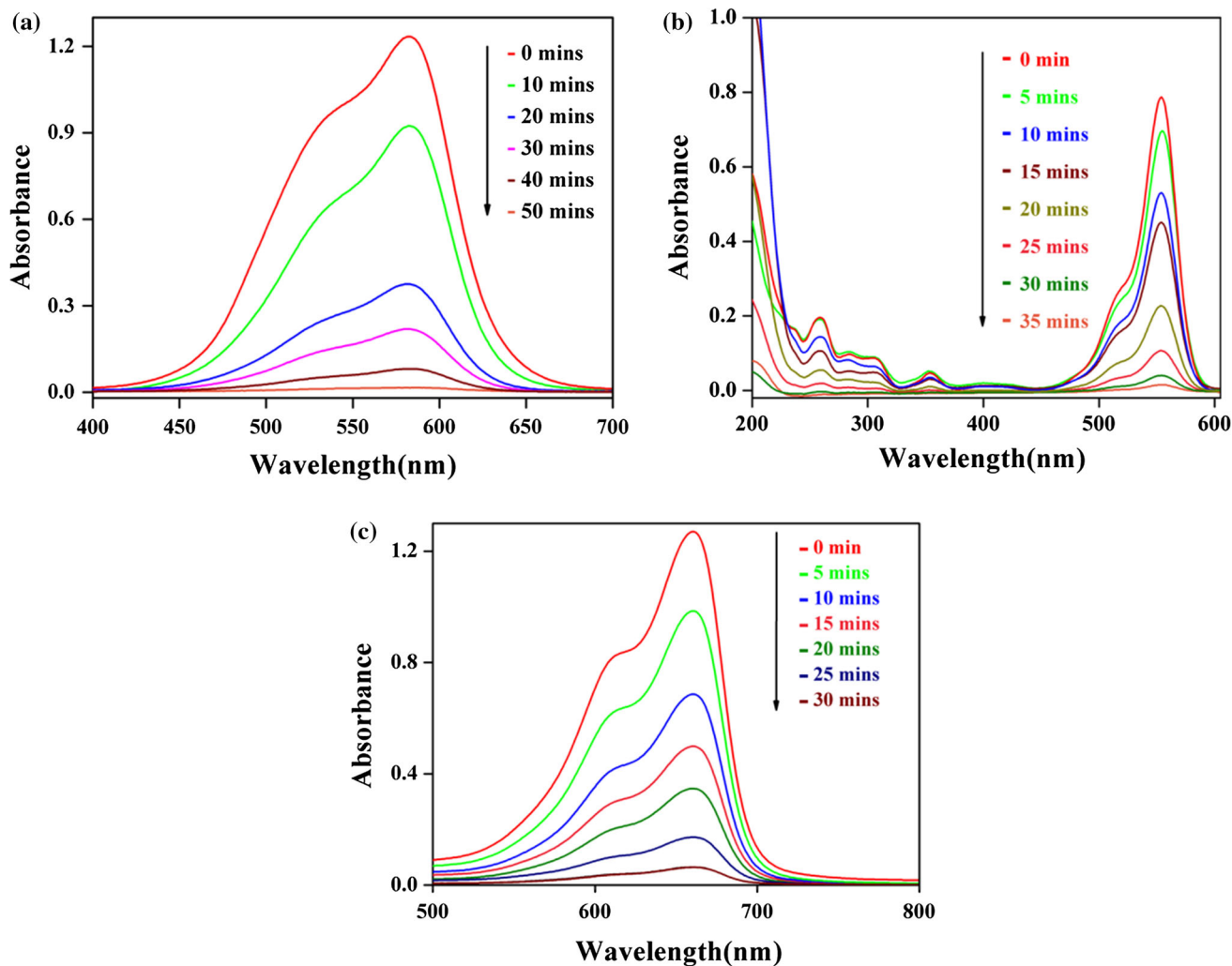
Fig. 5 Absorption spectra of **a** CV, **b** RhB and **c** MB dye solutions under UV light irradiation in the presence of 50 mg of NiO nanospheres

two dye solutions were degraded within 35 min, while the main absorption peak of the dye solution was decreased and reached almost zero.

3.5 Comparison of the photocatalytic activity

For the evaluation of the photocatalytic efficiency of NiO nanospheres towards the removal of CV, TiO_2 P25 and commercial NiO were selected as the reference under the identical reaction conditions which are shown Fig. 6. The degradation percentiles were 98, 81 and 61 for NiO nanospheres, TiO_2 P25 and commercial NiO, respectively, at 60 min irradiation time under UV light irradiation. The comparison results of the photocatalytic experiments indicated that NiO nanospheres increase the degradation rate of CV significantly. This distinguished behaviour of NiO nanospheres may be attributed to the tailored band gap, large surface area and high crystalline nature, which
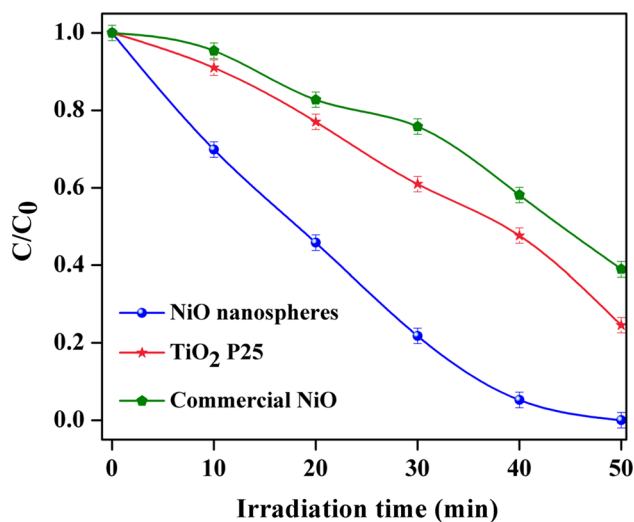

Fig. 6 Photodegradation of CV dye solutions with different photocatalysts under UV light irradiation

significantly facilitated the diffusion and mass transportation of CV molecules and delayed the recombination rate of photogenerated electron–hole pairs in the photocatalysis process. In general, defects in catalysts structure play a significant role in photocatalysis because the oxygen defects could also effectively separate the electron–hole pairs evolved during the photocatalytic process [29].

To understand the photogenerated electron–hole pairs separation and the electrons transfer performance, the photoluminescence spectrum for NiO nanospheres was examined as shown Fig. 7. The PL emission of NiO nanospheres was observed in the region of 350 nm, and the emission in the UV region is attributed to the recombination between electrons in conduction band and holes in valence band which takes place in the UV region. The visible emission is related to the defects -related deep level emission such as oxygen vacancies and Ni-interstitials [4]. Finally, there are a weak and a broad visible emission band at 525 nm that is usually attributed to native defects such as Ni-interstitials and O vacancies. PL emission is mainly due to the recombination of excited electrons and photogenerated holes in the semiconductor. The stronger the PL intensity is, the faster the photoexcited electron–hole pair. Generally, a higher PL intensity indicates a higher recombination rate, a lower PL intensity expresses and a lower recombination rate [30]. The emission of NiO nanospheres had very low intensity which clearly indicates the slower recombination rate of NiO nanospheres. For the prepared NiO nanospheres, the bandgap energy was 3.31 eV and commercial NiO has the bandgap energy of 3.45–4.5 eV, which clearly indicated that the band gap of NiO nanospheres decreased when compared to commercial NiO due to the excess oxygen vacancies, resulting from the elimination of the hydroxyl groups during the thermal
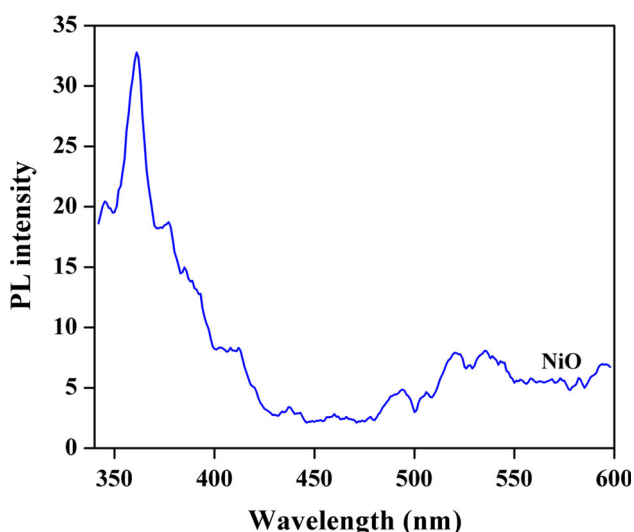
treatment of NiO nanospheres. By comparing this all technical properties, as-prepared NiO nanospheres could be a promising photocatalyst for the degradation of many organic contaminants.

3.6 Detection of reactive oxidative species (ROS)

In general, the photocatalytic reaction led by holes (h^+), electrons (e^-), hydroxyl radical ($^.OH$) and superoxide radical anion $O_2^{.-}$. The involvement of ROS in the photocatalytic reaction was investigated by trapping experiment using different scavenger as shown in Fig. 8. To probe the involvement of h^+ in the photocatalytic reaction, ammonium oxalate (AO), a well-known scavenger for h^+, was used [31–33]. The rate of photocatalytic degradation of the present system was not affected in the presence of AO, which could clearly support the involvement of h^+ which precedes the photocatalytic reaction. Hydroquinone (HQ) and azide ion (AZ) slowdown the photocatalytic degradation rate which clearly evident that the photocatalytic reaction precedes by the formation of $O_2^{.-}$ [34, 35]. Here, the rate of the photocatalytic degradation was not changed much which may be due to the absence of $O_2^{.-}$. TPP suppress the photocatalytic reaction that could clearly confirm the presence of $O_2^{.-}$ in the photocatalytic degradation reaction.

3.7 Plausible mechanism of degradation

In general, high activity of the photocatalyst should satisfy two requirements viz large surface area for absorbing photons and high crystallinity to reduce photo-excited electron–hole recombination rate. The photocatalytic reaction may involve the following steps
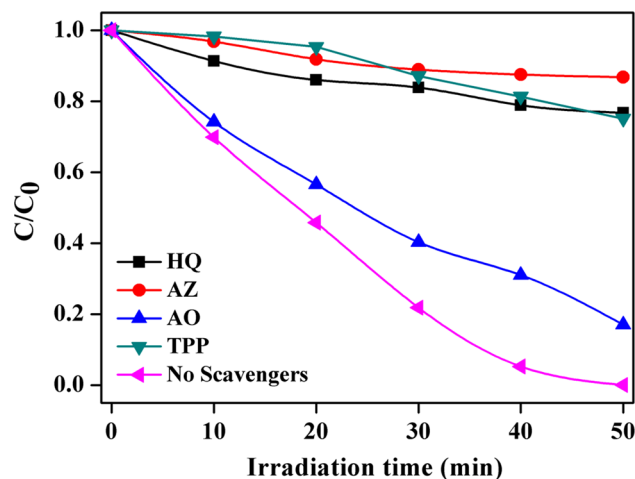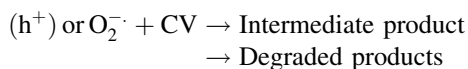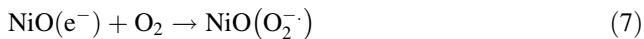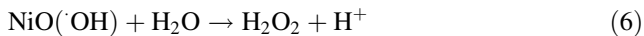
Fig. 7 PL emission spectrum of NiO nanospheres

Fig. 8 Effect of different scavengers on the photodegradation of CV dye solutions

$$NiO + h\nu \rightarrow NiO(e^- + h^+) \tag{3}$$

$$NiO(h^+) + H_2O \rightarrow NiO(^\cdot OH) + H^+ \tag{4}$$

$$NiO(h^+) + OH^- \rightarrow NiO(^\cdot OH) + H^+ \tag{5}$$

$$NiO(^\cdot OH) + H_2O \rightarrow H_2O_2 + H^+ \tag{6}$$

$$NiO(e^-) + O_2 \rightarrow NiO(O_2^- \cdot) \tag{7}$$

$$(h^+) \text{ or } O_2^- \cdot + CV \rightarrow \text{Intermediate product}$$
$$\rightarrow \text{Degraded products}$$
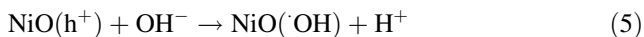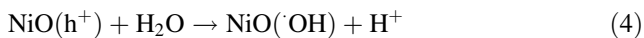
The semiconductor photocatalysis was based on the generation of the electron (e^-)–hole (h^+) pair under UV light irradiation. Upon UV light irradiation, the electron excited and migrated from the valence band to the conduction band, leaving a hole behind in the valence band (Eq. 3). Subsequently, the charge separation is maintained, and the electron and hole could migrate to the semiconductor surfaces where they participate in redox reactions with the adsorbed organic species [36]. Moreover, h^+ formed in the VB adsorbed water molecule and forms the hydroxyl radical which could react further to form an oxidizing agent (Eq. 4–6). The e^- in the CB adsorbed O_2 molecule, and superoxide is formed (Eq. 5). Then, formed ROS was degraded the dye molecules.

The higher crystallinity leads to the reduction of crystal defects in the crystal structure, which would result into the decrease in the recombination chance of photo induced carriers. Hence, the higher photocatalytic activity can be ascribed to the improved separation rate of photo induced electron–hole pairs. However, although the crystallinity increases with the increase of heat treat temperature, the decrease of photocatalytic activity can be ascribed to the reduced surface area. It is well known that porous structure shows better adsorption ability than solid materials, and the dye molecules and radicals can be effectively adsorbed on their surface, which results in the promotion for the photocatalytic process [20]. On the other hand, more active site on the surface of porous structure may accelerate the occurrence of photocatalytic reaction.

4 Conclusion

Bandgap-tailored NiO nanospheres were successfully synthesized by simple precipitation method and characterized using UV, FTIR, XRD, SEM, EDX, TEM and PL. The as-synthesized NiO nanospheres were showed sphere like structure which had smooth surface, and the particle size is 20 nm. The XRD result confirms that the NiO nanospheres were highly crystalline and cubic phase with an average crystallite size of 44 nm. The photocatalytic activity of the NiO was evaluated towards the degradation

of CV dye, and the complete degradation of the dye solution was observed within 50 min. The efficiency of the as-prepared NiO nanospheres was compared with commercial NiO and TiO_2 P25, and the corresponding degradation percentage is 98, 81 and 61 %, respectively. Effect of scavengers experiment used to predict the mechanism path and superoxide radical anion (O_2^-) and holes (h^+) was involved in the photodegradation. Since this process involves low toxicity, it does not need any oxidant and utilizes UV light and environment-friendly process.

References

1. H.J. Fan, C.S. Lu, W.L.W. Lee, M.R. Chiou, C.C. Chen, J. Hazard. Mater. **185**, 227 (2011)
2. R. Ahmad, J. Hazard. Mater. **171**, 767 (2009)
3. P.S. Kumar, M. Selvakumar, P. Bhagabati, B. Bharathi, S. Karuthapandian, S. Balakumar, RSC Adv. **4**, 32977 (2014)
4. S.G. Babu, R. Vinoth, P.S. Narayana, D. Bahnemann, B. Neppolian, APL Mater. **3**, 104415 (2015)
5. A. Nezamzadeh-Ejhieh, Z. Banan, Desalination **284**, 157 (2012)
6. C.C. Chen, H.J. Fan, C.Y. Jang, J.L. Jan, H.D. Lin, C.S. Lu, J. Photochem. Photobiol. A **184**, 147 (2006)
7. K.P. Singh, S. Gupta, A.K. Singh, S. Sinh, J. Hazard. Mater. **186**, 1462 (2011)
8. Y. Jua, J. Fang, X. Liu, Z. Xu, X. Ren, C. Sun, S. Yang, Q. Ren, Y. Ding, K. Yu, L. Wang, Z. Wei, J. Hazard. Mater. **185**, 1489 (2011)
9. C. Domingo, T.D.L. Arcos, A. Ainestschian, M.M. Sanz, I. Tanarro, Vib. Spectrosc. **30**, 157 (2002)
10. C. Guillard, D. Baldassare, C. Duchamp, M.N. Ghazzal, S. Daniele, Catal. Today **122**, 160 (2007)
11. K. Ito, T. Tomino, M. Ohshima, H. Kurakawa, K. Sugiyama, H. Miura, Appl. Catal. A **249**, 19 (2003)
12. L.R. Bentley, T.G. Chasteen, Chemosphere **55**, 291 (2004)
13. J.M.M. Zwart, J.G. Keunen, C_1-cycle of sulfur compounds. Biodegradation **3**, 37 (1992)
14. W. Au, S. Pathak, C.I. Collie, T.S. Hsu, Mutat. Res. **58**, 269 (1978)
15. A.Y. Zahrim, N. Hilal, Water Resour. Ind. **3**, 23 (2013)
16. N. Ghaemi, S.S. Madaeni, P. Daraei, H. Rajabi, T. Hojaeimehr, F. Rahimpour, B. Shirvani, J. Hazard. Mater. **298**, 111 (2015)
17. A. Bhatnagar, W. Hogland, M. Marques, M. Sillanpaa, Chem. Eng. J. **219**, 499 (2013)
18. V.K. Gupta, I.A.T.A. Saleh, A. Nayak, S. Agarwal, RSC Adv. **2**, 6380 (2012)
19. S.G. Babu, R. Vinoth, D.P. Kumar, M.V. Shankar, H.L. Chou, K. Vinodgopal, B. Neppolian, Nanoscale **7**, 7849 (2015)
20. K. Saravanakumar, M.M. Ramjan, P. Suresh, V. Muthuraj, J. Alloys Compd. **664**, 149 (2016)
21. Y. Ju-Na, J.R. Lead, Sci. Total Environ. **400**, 396 (2008)
22. D.H. Yang, C.S. Park, J.H. Min, M.H. Oh, Y.S. Yoon, S.W. Lee, J.S. Shin, Curr. Appl. Phys. **9**, 132 (2009)

23. F. Augusto, E. Carasek, R. Gomes Costa Silva, S.R. Rivellino, A.D. Batista, E.A. Martendal, J. Chromatogr. A **1217**, 2533 (2010)
24. A. Molla, M. Sahu, S. Hussain, J. Mater. Chem. A **3**, 15616 (2015)
25. A. Molla, M. Sahu, S. Hussain, Sci. Rep. **6**, 26034 (2016)
26. B. Bharathi, S. Thanikaikarasan, P. Kollu, P.V. Chandrasekar, K. Sankaranarayanan, X. Sahaya Shajan, J. Mater. Sci. **12**, 5338 (2014)
27. S.C. Lyu, Y. Zhang, H. Ruh, H.J. Lee, H.W. Shem, E. Esuh, Chem. Phys. Lett. **363**, 134 (2002)
28. H. He, S. Yang, K. Yu, Y. Ju, C. Sun, L. Wang, J. Hazard. Mater. **173**, 393 (2010)
29. P.S. Kumar, M. Selvakumar, S.G. Babu, S. Karuthapandian, S. Chattopadhyay, Mater. Lett. **151**, 45 (2015)
30. C. Karunakaran, S. Senthilvelan, S. Karuthapandian, Sol. Energy Mater. Sol. Cells **89**, 391 (2005)
31. P.S. Kumar, M. Selvakumar, S.G. Babu, S.K. Jaganathan, S. Karuthapandian, S. Chattopadhyay, RSC Adv. **5**, 57493 (2015)
32. S.G. Babu, R. Vinoth, B. Neppolian, D.D. Dionysiou, M. Ashokkumar, J. Hazard. Mater. **291**, 83 (2015)
33. P.S. Kumar, S. Karuthapandian, M. Umadevi, A. Elangovan, V. Muthuraj, Mater. Focus **5**, 128 (2016)
34. P. Latha, R. Dhanabackialakshmi, P.S. Kumar, S. Karuthapandian, Sep. Purif. Technol. **168**, 124 (2016)
35. P. Karthik, R. Vinoth, S.G. Babu, M. Wen, T. Kamegawa, H. Yamashita, B. Neppolian, RSC Adv. **5**, 39752 (2015)
36. C. Karunakaran, S. Karuthapandian, Sol. Energy Mater. Sol. Cells **90**, 1723 (2006)